Computational efficiency assessment of pin-by-pin SP_3 solvers under a unified response matrix formulation

Sicheng Wang, Ser Gi Hong *
Department of Nuclear Engineering, Hanyang University
**Corresponding author: sergihong@hanyang.ac.kr*

***Keywords :** Pin-by-pin; SP_3 theory; FDM; NEM; EFEN*

1. Introduction

As the demand for precision in reactor core physics analysis increases, considering both computational costs and the resources available on current mainstream computing platforms, pin-by-pin calculation [1] has gradually become a hot topic of research. This scheme can provide the pin-wise distributions of the parameters while eliminating errors caused by the assembly homogenization and pin-power reconstruction used in classical assembly-wise nodal methods.

Besides, direct diffusion approximation could be no more suitable considering the optical thickness of the refined pin-wise mesh and heterogeneities in advanced reactor cores. Usually, the pin-by-pin solvers employ the SP_3 transport approximation [2] to consider the transport effect with computational efficiency because the fully transport methods such as MOC still require a heavy computational burden.

In this paper, the response relationships between partial currents were proposed based on a unified response matrix formulation for different methods, including the finite difference method (FDM), exponential function expansion method (EFEN) [3], and nodal expansion methods (NEM) [4]. On this basis, the various solutions of the pin-by-pin multi-group SP_3 equations have been easily achieved under the same calculation process by selecting the corresponding response coefficients. Additionally, we evaluated the accuracy and efficiency of the above-mentioned methods through the 2D KAIST benchmark problem.

2. A Unified Response Matrix Formulation of Pin-by-pin SP3 Calculation

The fundamental of the response matrix solution of pin-by-pin SP_3 calculation is the derivation of the relationship of outgoing currents with the linear combination of the incoming current and average flux. By substituting the relationship into the neutron balance equation, the solution of flux could be systematically obtained, and the partial currents could be updated in the inner iteration directly, eliminating the requirement of nonlinear iterations [5]. Another benefit from the incoming partial current-related formulation is the fact that the spatial mesh sweeping could employ a Jacobi sweeping (sweep all the meshes together) or the red-black Gauss-Siedel sweeping (sweep half of the meshes together each inner iteration) easily, which will lead to the further efficient parallelization.

2.1 Basic equations in the SP_3 theory

The traditional form of the SP_3 equations with isotropic scattering is shown as follows:

$$\begin{cases} m=0: \\ -D_g\nabla^2\left(\varphi_g^0+2\varphi_g^2\right)+\Sigma_{r,g}\left(\varphi_g^0+2\varphi_g^2\right)=S_g+2\Sigma_{r,g}\varphi_g^2 \\ m=2: \\ -\frac{27}{35}D_g\nabla^2\varphi_g^2+\Sigma_{t,g}\varphi_g^2=\frac{2}{5}\left(\Sigma_{r,g}\varphi_g^0-S_g\right) \end{cases} \quad (1)$$

If the following definitions are implemented

$$\begin{cases} \phi_g^0=\varphi_g^0+2\varphi_g^2, \phi_g^2=\varphi_g^2 \qquad S_g^0=S_g+2\Sigma_{r,g}\phi_g^2, S_g^2=\frac{2}{5}\left(\Sigma_{r,g}\phi_g^0-S_g\right) \\ D_g^0=D_g, D_g^2=\frac{27}{35}D_g \qquad \Sigma_{tr,g}^0=\Sigma_{r,g}, \Sigma_{tr,g}^2=\Sigma_{t,g} \end{cases}, \quad (2)$$

then, $m=0$ and $m=2$ equations in Eq. (1) can be written as the same form of diffusion equation as

$$-D_g^m\nabla^2\phi_g^m+\Sigma_{tr,g}^m\phi_g^m=S_g^m. \quad (3)$$

It should be noted that differently from the direct diffusion equation, the two diffusion-like equations of the SP_3 theory (i.e., Eq.(3)) are coupled with each other. Besides, in the SP_3 theory, the partial current and net current of different orders could be defined as

$$\begin{cases} J_{g,u\pm}^{m,o}+J_{g,u\pm}^{m,i}=\frac{1}{2}\bar{\phi}_{g,u\pm}^m, \\ J_{g,u+}^{m,o}-J_{g,u+}^{m,i}=J_{g,u+}^{m,net}, \qquad -J_{g,u-}^{m,o}+J_{g,u-}^{m,i}=J_{g,u-}^{m,net} \end{cases}, \quad (4)$$

where the subscript u stands for the surface in Cartesian coordinate, and $u=x,y,z$; the superscript o stands for the out-going partial current, i stands for the in-coming partial current, and *net* stands for the net current. And the neutron balance equations of each order could be described as

$$\sum_{u=x,y,z}\frac{J_{g,u+}^{m,net}-J_{g,u-}^{m,net}}{h_u}+\Sigma_{tr,g}^m\bar{\phi}_g^m=\bar{S}_g^m. \quad (5)$$

2.2 Response relationship in FDM

In order to get the analytic solution of the diffusion-like equations shown in Eq.(3), first, the straightforward FDM approach is implemented, which also plays the role of a preliminary example of the solution scheme.

The key point of the FDM is the direct employment of Fick's Law as

$$J_{g,u+}^{m,net} = -D_g^m \frac{\phi_{g,u+}^m - \bar{\phi}_g^m}{h_u/2}, J_{g,u-}^{m,net} = -D_g^m \frac{\bar{\phi}_g^m - \phi_{g,u-}^m}{h_u/2}. \quad (6)$$

With this approximation, by substituting Eq.(6) into Eq.(4), it could be easy to obtain the following relationship as

$$J_{g,u\pm}^{m,o} = \mu_{g,u}^m J_{g,u\pm}^{m,i} + \eta_{g,u}^m \bar{\phi}_g^m, \quad (7)$$

where the coefficients $\mu_{g,u}^m$ and $\eta_{g,u}^m$ could be calculated with the given cross-sections and mesh length as

$$\mu_{g,u}^m = \frac{1-4\frac{D_g^m}{h_u}}{1+4\frac{D_g^m}{h_u}}, \eta_{g,u}^m = \frac{2\frac{D_g^m}{h_u}}{1+4\frac{D_g^m}{h_u}}. \quad (8)$$

By substituting this response relationship Eq.(8) into the neutron balance equation Eq.(5), the balance equation becomes

$$\left(2\sum_{u=x,y,z}\frac{\eta_{g,u}^m}{h_u} + \Sigma_{tr,g}^m\right)\bar{\phi}_g^m + \sum_{u=x,y,z}\frac{\mu_{g,u}^m - 1}{h_u}\left(J_{g,u+}^{m,i} + J_{g,u-}^{m,i}\right) = \bar{S}_g^m. \quad (9)$$

Here in Eq.(9), the average flux is only related to the in-coming partial currents. With the initial $J_{g,u\pm}^{m,i}$, the average flux could be updated. The detailed solution process will be discussed in Section 2.5.

2.3 Response relationship in EFEN

Regarding FDM, since there is just a simple spatial assumption in space discretization, it could only obtain good accuracy when the mesh size is sufficiently small, resulting in it being a quite expansive method in the practical PWR neutronics analysis.

Hence the nodal method is viewed as a good choice for the pin-by-pin SP_3 calculation. Among them, the EFEN [6] (or called ACMFD [7]) method with the flat source and flat leakage approximation has been implemented in some well-developed pin-by-pin codes.

With the flat source and leakage approximations, Eq.(3) is a typical Helmholtz Equation, therefore, the analytic solution of the transverse flux with the flat source and leakage approximations could be expressed as

$$\phi_{ug}^m(u) = Ae^{\kappa_g^m u} + Be^{-\kappa_g^m u} + \frac{R_{g,u}^m}{D_g^m\left(\kappa_g^m\right)^2}, u \in \left[-\frac{h_u}{2}, \frac{h_u}{2}\right]$$

$$\text{where } R_{g,u}^m = \bar{S}_g^m - \bar{L}_{g,v}^m - \bar{L}_{g,w}^m \quad (10)$$

$$\bar{L}_{g,v}^m = \frac{J_{g,v+}^{m,net} - J_{g,v-}^{m,net}}{h_v}, \bar{L}_{g,w}^m = \frac{J_{g,w+}^{m,net} - J_{g,w-}^{m,net}}{h_w}$$

With this analytic expression and the basic equations shown in Section 2.1, the response relationship in EFEN could be derived as

$$J_{g,u\pm}^{m,o} = \mu_{g,u}^m J_{g,u\pm}^{m,i} + \eta_{g,u}^m \bar{\phi}_g^m + \theta_{g,u}^m. \quad (11)$$

The expressions of the coefficients are shown in Eq.(12). It should be pointed out that with the limit $h_u \to 0$, the coefficients in Eq.(12) would degenerate to those obtained from the FDM in Eq.(8) according to the L'Hôpital's rule. Hence the coefficient $\theta_{g,u}^m$ can be considered as a spatial correction factor compared to the FDM method.

$$\begin{cases} \mu_{g,u}^m = \dfrac{-2D_g^m\kappa_g^m\left(e^{\kappa_g^m h_u} - e^{-\kappa_g^m h_u}\right) + \left(e^{\kappa_g^m h_u} + e^{-\kappa_g^m h_u}\right) - 2}{2D_g^m\kappa_g^m\left(e^{\kappa_g^m h_u} - e^{-\kappa_g^m h_u}\right) + \left(e^{\kappa_g^m h_u} + e^{-\kappa_g^m h_u}\right) - 2} \\ \eta_{g,u}^m = \dfrac{2h_x D_g^m\left(\kappa_g^m\right)^2}{2D_g^m\kappa_g^m\left(e^{\kappa_g^m h_u} - e^{-\kappa_g^m h_u}\right) + \left(e^{\kappa_g^m h_u} + e^{-\kappa_g^m h_u}\right) - 2} \\ \theta_{g,u}^m = \dfrac{\left(e^{\kappa_g^m h_u} - e^{-\kappa_g^m h_u} - 2\kappa_g^m h_u\right)R_{g,u}^m}{2D_g^m\left(\kappa_g^m\right)^2\left(e^{\kappa_g^m h_u} - e^{-\kappa_g^m h_u}\right) + \kappa_g^m\left(e^{\kappa_g^m h_u} + e^{-\kappa_g^m h_u}\right) - 2\kappa_g^m} \end{cases} \quad (12)$$

2.4 Response relationship in NEM

Even though EFEN could achieve a significant improvement in accuracy than the FDM, due to its flat source approximation, it still meets challenges in systems with dramatic changes in neutron spectrum such as partially loaded MOX cores.

One approach that could overcome this issue is the nodal expansion method. Usually, the transverse flux and the corresponding transverse source term in NEM employ the 4th-order expansion and the transverse leakage term employs the quadratic approximation as

$$\begin{cases} \phi_{ug}^m(u) = \bar{\phi}_g^m + \sum_{n=1}^4 \alpha_{ug,n}^m f_n(u) \\ S_{ug}^m(u) = F(\phi_{ug}^m(u)) \\ L_{ug,v}^m(u) = \bar{L}_{g,v}^{m,l} + b_{xg,v,1}^m f_1(u) + b_{xg,v,2}^m f_2(u) \end{cases} \quad (13)$$

In order to introduce the advantages of the response matrix method into NEM as well, the partial current response relationship of the NEM is derived from Eq.(13) with the weighted residual moment method as

$$\begin{cases} J_{g,u+}^{m,o} = \left(\mu_{g,u}^m - \nu_{g,u}^m\right)J_{g,u+}^{m,i} + \nu_{g,u}^m J_{g,u-}^{m,i} + \eta_{g,u}^m\bar{\phi}_g^m + \theta_{g,u}^m + \zeta_{g,u}^m \\ J_{g,u-}^{m,o} = \left(\mu_{g,u}^m - \nu_{g,u}^m\right)J_{g,u-}^{m,i} + \nu_{g,u}^m J_{g,u+}^{m,i} + \eta_{g,u}^m\bar{\phi}_g^m + \theta_{g,u}^m - \zeta_{g,u}^m \end{cases} \quad (14)$$

The expressions of the coefficients are shown in APPENDIX. It could be noted here that differently from the FDM and EFEN, the out-going partial current of $u+$ surface $J_{g,u+}^{m,o}$ is not only related to the in-coming partial current of the same surface $J_{g,u+}^{m,i}$, but also the in-coming partial current of the opposite surface $J_{g,u-}^{m,i}$.

Besides, the influence of the expansion of the source term and leakage term is reflected in the moment term shown in $\theta_{g,u}^m$ and $\zeta_{g,u}^m$. Hence, these coefficients could be viewed as high-order correction factors compared to the FDM and EFEN methods.

2.5 Unified Response Matrix Formulation of SP_3 equations and solver development

Similarly to Eq.(9), by substituting the EFEN response relationship Eq.(11) or the NEM response

relationship Eq.(14) into the neutron balance equation Eq.(5), it could be transformed into

$$\left(2\sum_{u=x,y,z}\frac{\eta_{g,u}^{m}}{h_u}+\Sigma_{tr,g}^{m}\right)\bar{\phi}_g^{m}+\sum_{u=x,y,z}\frac{\mu_{g,u}^{m}-1}{h_u}\left(J_{g,u+}^{m,i}+J_{g,u-}^{m,i}\right)+\sum_{u=x,y,z}\frac{\theta_{g,u}^{m}}{h_u}=\bar{S}_g^{m} \tag{15}$$

or the response matrix formulation when we take Eq.(2) into account as

$$\begin{bmatrix}\Sigma_{r,g}+2H_g^0 & 4H_g^0\\ -\frac{2}{5}\Sigma_{r,g} & \Sigma_{t,g}+2H_g^2\end{bmatrix}\begin{bmatrix}\bar{\varphi}_g^{0}\\ \bar{\varphi}_g^{2}\end{bmatrix}=\begin{bmatrix}S_g-U_g^0-2L_g^0\\ -\frac{2}{5}S_g-U_g^2-2L_g^2\end{bmatrix} \tag{16}$$

where

$$\begin{cases}H_g^m=\sum_{u=x,y,z}\frac{\eta_{g,u}^{m}}{h_u}, \qquad L_g^m=\sum_{u=x,y,z}\frac{\theta_{g,u}^{m}}{h_u}\\ U_g^m=\sum_{u=x,y,z}\frac{\mu_{g,u}^{m}-1}{h_u}\left(J_{g,u+}^{m,i}+J_{g,u-}^{m,i}\right)\end{cases} \tag{17}$$

It demonstrates all FDM, EFEN, and NEM solutions of the SP_3 equations could be unified under the same response matrix formulation as shown in Eq.(17).

In the practical solution, under a given source term, the average flux could be updated with the initial in-coming partial current. With the response relationships, the out-going partial current could be updated then. Considering the continuity of the partial currents, the out-going partial currents could be used to update the neighbor meshes' in-coming partial currents. The above steps will be iterated in the inner iteration until convergence.

Based on the solution process, the pin-by-pin SP_3 solvers have been developed. The one-node CMFD method is also implemented in the solver, which employs the partial-current-based analytic solution shown in Eq.(16) to solve the coarse mesh balance equations. Considering that the switch of different solvers only has an influence on the inner iteration, those solvers share the same outer iteration module and CMFD acceleration module, which are both independent of the inner iteration module.

3. Verifications based on the 2D KAIST benchmark

The 2D KAIST 3A benchmark problem [8] is used to evaluate different methods, which provides 7-group pin-cell homogenized cross sections, including UOX and MOX fuel rods, control rods, and poison rods. The core layout of the 2D KAIST 3A benchmark is shown in Fig. 1.

Homogenized pin cell is divided into 1x1 and 2x2 meshes per pin-cell respectively. The mesh-independent reference solution is calculated by FMFD with 10x10 mesh per pin cell. The sensitivity analysis results on pin and assembly powers including eigenvalue by mesh divisions are given in Table I and Table II, while the detailed relative discrepancies of pin-wise power from the reference refined FDM values are shown in Fig. 2 and Fig. 3. It could be noted that the scale of the color bar of FDM is different from the others in Fig. 2 and Fig. 3 due to its large values in the magnitude of discrepancy from the refined reference FDM solution. Besides, the calculation time and number of outer iterations are also shown in Table III.

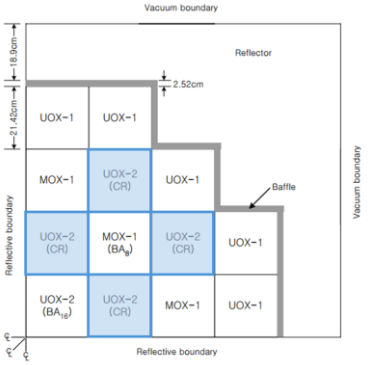

Fig. 1. Core layout of 2D KAIST 3A benchmark

Table I: Relative discrepancies (%) of the pin and assembly powers with 1x1 mesh per pin-cell

	k_{eff} difference (pcm)	Assembly-wise power		Pin-wise power	
		RMS	MAX	RMS	MAX
FDM	1600	12.07	25.54	12.80	34.07
EFEN	-30	0.89	1.57	1.17	4.39
NEM	5	0.08	0.21	0.11	0.52

Table II: Relative discrepancies (%) of the pin and assembly powers with 2x2 meshes per pin-cell

	k_{eff} difference (pcm)	Assembly-wise power		Pin-wise power	
		RMS	MAX	RMS	MAX
FDM	542	4.33	9.25	4.59	11.94
EFEN	-2	0.25	0.43	0.35	1.15
NEM	-18	0.15	0.31	0.16	0.47

Table III: Computation cost of various methods

	Calculation time	Total number of outer iterations
FDM (1x1)	34.578s	26
EFEN (1x1)	42.673s	24
NEM (1x1)	87.905s	26
FDM (2x2)	201.246s	30
EFEN (2x2)	246.494s	26
NEM (2x2)	400.460s	26

It could be found from the results that the FDM solver is not suitable for the strong heterogeneity ARI case because the RMS of assembly power and pin power discrepancies are both about 5% even for the 2x2 calculation.

For the 1x1 EFEN calculation, which has the common mesh division in the pin-by-pin calculation, the RMS of assembly power discrepancies is less than 1%. However, the maximum discrepancy in pin power distribution is 4.39%, which is located at the boundary of the fuel assembly as shown in Fig. 2 where the flux spectrum changes dramatically.

As expected, the NEM solver could get the most accurate results for the ARI case. RMS of pin-wise power discrepancies is 0.11% and the maximum pin-wise power discrepancy is 0.52% for the 1x1 NEM

calculation, which is also better than the 2x2 EFEN calculation. With the employment of the refined 2x2 mesh, the accuracy could be improved as expected.

It could be indicated that the NEM method requires more computation time than EFEN since more coefficients are required for the solution. However, considering the accuracy, the 1x1 NEM is also more efficient than 2x2 EFEN, which could reduce the calculation time from 246s to 88s.

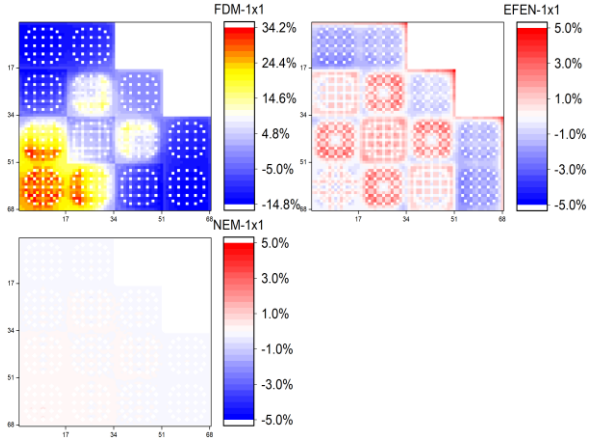

Fig. 2. Relative pin-power discrepancies (1x1 mesh per pin-cell)

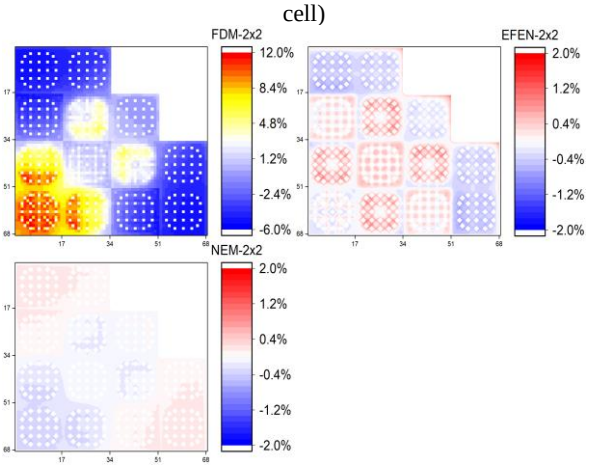

Fig. 3. Relative pin-power discrepancies (2x2 mesh per pin-cell)

4. Conclusions

In this paper, a partial-current-based unified response matrix formulation is employed to solve the pin-by-pin SP_3 equations with various methods including FDM, EFEN, and NEM. Benefiting from the unified solution process, the different methods could be implemented and switched easily and share the same outer iteration module and CMFD acceleration module.

The heterogenous 2D KAIST benchmark problem was used to evaluate the accuracy and efficiency of the solvers using the different methods. The comparison demonstrates that for the strong heterogeneous case, the NEM solver could provide the most accurate results due to the high-order source and leakage expansion compared to the EFEN and FDM solver. The RMS and maximum value of pin-power discrepancies of 1x1 NEM solver are both less than 1%, while EFEN requires at least 2x2 mesh per pin-cell with three times longer computing than the time of 1x1 NEM to achieve such accuracy.

REFERENCES

[1] Jaeha Kim and Yonghee Kim. Development of 3-D HCMFD algorithm for efficient pin-by-pin reactor analysis, Annals of Nuclear Energy, Vol. 127, pp. 87-09, 2019.
[2] A. M. Gomez-Torres, V. H. Sanchez-Espinoza, K. Ivanov, et al. DYNSUB: A high fidelity coupled code system for the evaluation of local safety parameters – Part I: Development, implementation, and verification, Annals of Nuclear Energy, Vol. 48, pp. 108-122, 2012.
[3] Yunzhao Li, Hongchun Wu, Liangzhi Cao. A polygonal nodal-SP3 method for whole core pin-by-pin calculation, M&C2011, Rio de Janeiro, Brazil, May 8-12, 2011.
[4] Seongho Song, Hwanyeal Yu, and Yonghee Kim. One-node and two-node hybrid coarse-mesh finite difference algorithm for efficient pin-by-pin core calculation, Nuclear Engineering and Technology, Vol. 50, pp. 327-339, 2018.
[5] YA Chao. A theoretical analysis of the coarse mesh finite difference representation in advanced nodal methods, Proc. Int. Conf. M&C'99, Vol. 1, p. 117, 1999.
[6] Yunzhao Li, Wen Yang, Sicheng Wang, et al. A 3D PWR-core Pin-by-pin analysis code NECP-Bamboo2.0, Annals of Nuclear Energy, Vol. 144: 107507, 2020.
[7] Masahiro TATSUMI and Akio YAMAMOTO. Advanced PWR Core Calculation Based on Multi-group Nodal-transport Method in Three-dimensional Pin-by-Pin Geometry, Journal of NUCLEAR SCIENCE and TECHNOLOGY, Vol. 40, No. 6, pp. 376–387, 2003.
[8] N. Z. Cho. KAIST Nuclear Reactor Analysis and Particle Transport Laboratory Benchmark Problem 1A, http://nurapt.kaist.ac.kr/benchmark.

APPENDIX

The coefficients of the NEM approach are expressed as

$$\begin{cases} \mu_{g,u}^m = \dfrac{1-M_{g,u}^m}{1+M_{g,u}^m}, \nu_{g,u}^m = \dfrac{N_{g,u}^m - M_{g,u}^m}{\left(1+M_{g,u}^m\right)\left(1+N_{g,u}^m\right)} \\ \eta_{g,u}^m = \dfrac{M_{g,u}^m}{2\left(1+M_{g,u}^m\right)} \\ \theta_{g,u}^m = \dfrac{P_{g,u}^m}{2\left(1+M_{g,u}^m\right)}, \zeta_{g,u}^m = \dfrac{Q_{g,u}^m}{2\left(1+N_{g,u}^m\right)} \end{cases} \quad \text{(A-1)}$$

where

$$\begin{cases} M_{g,u}^m = 4\dfrac{D_g^m}{h_u}\dfrac{10\Sigma_{tr,g}^m\left(h_u\right)^2 + 420D_g^m}{\Sigma_{tr,g}^m\left(h_u\right)^2 + 140D_g^m} \\ N_{g,u}^m = 4\dfrac{D_g^m}{h_u}\dfrac{6\Sigma_{tr,g}^m\left(h_u\right)^2 + 60D_g^m}{\Sigma_{tr,g}^m\left(h_u\right)^2 + 60D_g^m} \\ P_{g,u}^m = \dfrac{280D_g^m h_u\left(\left\langle \omega_2, S_{ug}^m\right\rangle - \dfrac{b_{ug,v,2}^m}{20h_v} - \dfrac{b_{ug,w,2}^m}{20h_w}\right)}{\Sigma_{tr,g}^m\left(h_x\right)^2 + 140D_g^m} \\ Q_{g,u}^m = \dfrac{120D_g^m h_u\left(\left\langle \omega_1, S_{ug}^m\right\rangle - \dfrac{b_{ug,v,1}^m}{12h_v} - \dfrac{b_{ug,w,1}^m}{12h_w}\right)}{\Sigma_{tr,g}^m\left(h_u\right)^2 + 60D_g^m} \end{cases} \quad \text{(A-2)}$$